Collective Modes in a Quantum Solid

Snir Gazit,[1,2] Daniel Podolsky,[2] Heloise Nonne,[2] Assa Auerbach,[2] and Daniel P. Arovas[3]

[1]*Department of Physics, University of California, Berkeley, California 94720, USA*
[2]*Physics Department, Technion, 32000 Haifa, Israel*
[3]*Department of Physics, University of California at San Diego, La Jolla, California 92093, USA*

We provide a theoretical explanation for the optical modes observed in inelastic neutron scattering on the bcc solid phase of helium 4 [T. Markovich *et al.*, Phys. Rev. Lett. **88**, 195301 (2002)]. We argue that these excitations are amplitude (Higgs) modes associated with fluctuations of the crystal order parameter *within* the unit cell. We present an analysis of the modes based on an effective Ginzburg-Landau model, classify them according to their symmetry properties, and compute their signature in inelastic neutron scattering experiments. In addition, we calculate the dynamical structure factor by means of an *ab intio* quantum Monte Carlo simulation and find a finite frequency excitation at zero relative momentum.

Introduction.—The harmonic theory of solids predicts that the excitation spectrum of a monoatomic Bravais lattice crystal should consist solely of acoustic phonons. It is therefore quite surprising that inelastic neutron scattering (INS) measurements have detected gapped opticlike modes in the bcc phase of solid helium 4 [1–3]. These gapped excitations include a dispersing longitudinal mode [1] and a nondispersing transverse mode [2–4]. Similar measurements carried out in the hcp phase of ^{4}He have tentatively identified opticlike modes *beyond* those expected for the hcp structure [5]. Previous theories associated these excitations with nonphononic dipolar [6–8] and delocalized vacancy modes [5]. These scenarios, while plausible, do not account for the existence of multiple gapped modes. Hence, a basic understanding of this phenomenon is still lacking.

In this Letter, we identify these optical excitations as amplitude modes of the solid order parameter. Amplitude ("Higgs") modes appear in many condensed matter systems and have recently been the focus of intense experimental and theoretical research. Some notable examples are superconductors [9–11], cold atoms in optical lattices [12,13], and antiferromagnets [14]. However, such modes are not generally expected in solids. Here we argue that the large zero-point fluctuations in solid ^{4}He allow it to be treated as a three-dimensional charge-density wave (CDW) that supports, in addition to the usual acoustic phonons, gapped amplitude modes.

The phonon spectrum of bcc ^{4}He depends strongly on quantum effects, and for two reasons. First, the classical bcc structure is difficult to stabilize with power law potentials, and for Lennard-Jones systems, the only equilibrium states are either hcp or fcc [15], at all molar volumes. Second, the small helium mass leads to large zero-point fluctuations on the order of 30% of the interatomic distance [16], well in excess of the Lindemann criterion. Although this does not

guarantee a melting transition [17], it provides an indication for the relatively strong density fluctuations in the bcc phase. This invalidates the use of real space atomic displacements as small expansion parameters, and entails significant nonlinear contributions to the equations of motion. To account for quantum fluctuations, Hartree [18] and self-consistent harmonic theories [19–22] have been used with general success to describe the experimentally observed acoustic phonon spectra [23,24]. If strong enough, the nonlinear quantum lattice dynamics can, in principle, support excitations beyond the acoustic phonons [25]. Physically, the large zero-point motion may allow for density fluctuations *within* the unit cell, which are likely responsible for the optical modes seen in neutron scattering.

A natural question is then how to construct a linear theory for the excitations of bcc ^{4}He. To address this problem, we note that the large spread of the atomic density profile within the unit cell leads to suppression of high lattice harmonics. This is in sharp contrast to the classical picture of a crystal with well-localized atoms, for which *all* lattice harmonics are sizable. It may therefore be justified to neglect high harmonics and consider only the Fourier weight corresponding to the primary Bragg vectors. The resulting description of the solid is then in terms of a CDW, whose spectrum naturally contains both acoustic phonons and amplitude modes (see Fig. 1).

Ginzburg-Landau (GL) theory.—In constructing the phenomenological Ginzburg-Landau theory we make two main assumptions. First, the gapped modes are presumed to result from density fluctuations (and not, e.g., from fluctuations related to nearby superfluid order). Second, we assume the density dynamics is dominated by a small number of primary Bragg vectors. Our results follow from these assumptions combined with symmetry considerations. Hence, we expect them to be robust and apply beyond the specific choice of the phenomenological model used.
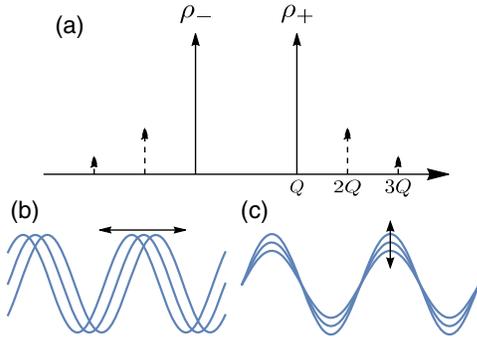
FIG. 1.   (a) A one-dimensional CDW is modulated at primary Bragg vectors $\pm Q$, with Fourier amplitudes $\rho_\pm$. Higher harmonics are strongly suppressed. Real space oscillations of (b) the acoustic phonon and (c) the amplitude mode.

For a solid with large density fluctuations, the GL free-energy functional can be written as an expansion in powers of the deviation of the particle density from its average value, $\delta\rho(r) = \rho(r) - \rho_0$ [26,27],

$$\mathcal{F}_{\mathrm{GL}}[\delta\rho(\boldsymbol{r})] = \int d^3r\, d^3r'\, \delta\rho(\boldsymbol{r}')\chi^{-1}(\boldsymbol{r}-\boldsymbol{r}')\,\delta\rho(\boldsymbol{r})$$
$$- B\int d^3r[\delta\rho(\boldsymbol{r})]^3 + C\int d^3r[\delta\rho(\boldsymbol{r})]^4. \quad (1)$$

The charge susceptibility kernel $\chi(\boldsymbol{r}-\boldsymbol{r}')$ must respect the underlying rotational symmetry and support an instability towards a CDW at a Bragg vector of magnitude G. These considerations are fulfilled by taking

$$\chi^{-1}(\boldsymbol{r}-\boldsymbol{r}') = \frac{1}{2}[R + v^2(\nabla^2 + G^2)^2]\delta(\boldsymbol{r}-\boldsymbol{r}'), \quad (2)$$

for which the quadratic term in Eq. (1) is minimized for all wave vectors $\boldsymbol{Q}$ of length G. For $R < 0$, any Fourier component of the density with $|\boldsymbol{Q}| = G$ contributes a negative free energy, thus leading to a CDW instability. The wave vector pattern $\{\boldsymbol{Q}_i\}$ selected is then determined by higher order terms in $\mathcal{F}_{\mathrm{GL}}$.

As shown in Refs. [26,27], the cubic term in $\mathcal{F}_{\mathrm{GL}}$ prefers structures that maximize the number of equilateral triangles which can be formed from the $\{\boldsymbol{Q}_i\}$. For three-dimensional crystals, this selects fcc in reciprocal space, hence bcc in real space. The density profile of the CDW is then $\delta\rho_{\mathrm{CDW}}(r) = \sum_{\boldsymbol{G}}\rho_{\boldsymbol{G}}e^{i\boldsymbol{G}\cdot\boldsymbol{r}}$, where the sum runs over the 12 primary Bragg vectors of the bcc lattice. Since $\rho(r)$ is real, we must have $\rho_{\boldsymbol{G}} = \rho_{-\boldsymbol{G}}^*$; hence, the total number of real degrees of freedom is 12, as opposed to three in the harmonic lattice theory. For the minimum energy configuration, $\rho_{\boldsymbol{G}}$ can be chosen to take a uniform ($\boldsymbol{G}$-independent) mean-field value $\rho_{\boldsymbol{G}} = \delta\bar{\rho}$. Excitations are then obtained by studying dynamical fluctuations of the density about the mean-field solution.

Excitation spectrum.—In order to study excitations, we consider the time-dependent GL Lagrangian density

$$\mathcal{L} = \frac{1}{\gamma}\left(\frac{\partial\delta\rho(\boldsymbol{r},t)}{\partial t}\right)^2 - \mathcal{F}_{\mathrm{GL}}[\delta\rho(\boldsymbol{r},t)], \quad (3)$$

where $\mathcal{F}_{\mathrm{GL}}$ is the free energy defined in Eq. (1). Note that since the density is real, $(\partial_t\rho)^2$ is the lowest order dynamical term that can be constructed. In principle, dissipative terms involving first order time derivatives are also allowed. These terms originate from processes in which gapped modes decay to acoustic phonons and lead to broadening of the line shapes. Experimentally, the modes are found to be sharp and hence we will neglect this effect in our phenomenological approach.

The excitation spectrum is obtained by linearizing the Euler-Lagrange equations with respect to the fluctuations $\eta_{\boldsymbol{G}}(q,\omega) = \rho(\boldsymbol{G}+q,\omega) - \delta\bar{\rho}$. Diagonalizing the resulting bilinear form yields the linear mode eigenfrequencies ω_α and eigenvectors $\boldsymbol{\xi}_\alpha$, as discussed in the Supplemental Material (SM) [28]. The longitudinal and transverse excitation spectrum in the vicinity of a principal Bragg vector is shown in Figs. 2(a) and 2(b). In addition to the three acoustic phonon branches, the spectrum also contains nine gapped optical modes.

Symmetry classification.—At zero relative momentum, $q = 0$, the normal modes can be classified according to irreducible representations (irreps) of the octohedral group O_h. In Fig. 2(a) we label the different modes according to their irreps. We find that the two lowest gapped modes are one s-wave and three d-wave T_{2g} modes. When the GL parameter R is below a critical value R^*, the d-wave mode is lower in energy than the s-wave modes; this order is exchanged for $R > R^*$. This is the only qualitative feature of our analysis that depends on the precise value of the GL parameters.

Interestingly, the d_{xy} mode is approximately dispersionless in the transverse direction, $\boldsymbol{q} = q\hat{z}$, as seen in Fig. 2(b). This behavior, seen experimentally [2,3], can be traced back to the reciprocal space structure of the
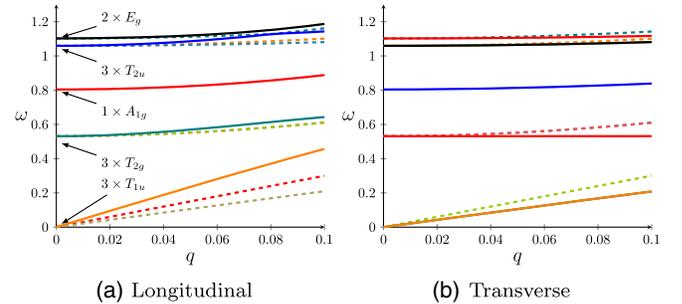

(a) Longitudinal   (b) Transverse

FIG. 2.   Excitation spectrum for the GL theory of bcc ^{4}He. GL parameters are chosen as $R = 0.05$, $B = C = 1$, and $v = 1.5$. The momentum transfer $\boldsymbol{q}$ is chosen relative to the principal Bragg vector $G = \{1,1,0\}$ in the (a) longitudinal $\boldsymbol{q} = (q,q,0)$ and (b) transverse $\boldsymbol{q} = (0,0,q)$ directions. Solid (dashed) lines correspond to INS active (inactive) modes. Modes labeled in (a) by their irreps and mode degeneracies at $q = 0$.
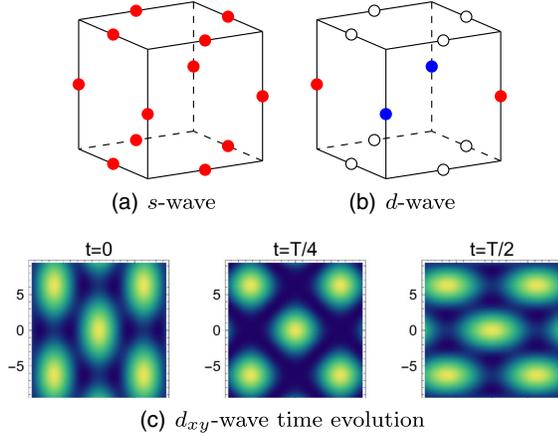
(a) *s*-wave   (b) *d*-wave

t=0   t=T/4   t=T/2

(c) d_{xy}-wave time evolution

FIG. 3. Reciprocal space structure of the (a) *s*-wave and (b) *d*-wave normal modes at the primitive Bragg vector. Red (blue) dots correspond to positive (negative) amplitudes η_G. (c) Real space evolution of the density for the d_{xy} mode at $q = 0$, at different instants in time.

mode depicted in Fig. 3, which has nonvanishing amplitude η_G only for $\boldsymbol{G}$ in the $z = 0$ plane. As a result, $\boldsymbol{G} \cdot \boldsymbol{q} = 0$, and the charge susceptibility kernel $\tilde{\chi}^{-1}(\boldsymbol{G}+\boldsymbol{q}) = \frac{1}{2}R + \frac{1}{2}v^2[(\boldsymbol{G}+\boldsymbol{q})^2 - G^2]^2 = \frac{1}{2}(R + v^2 q^4)$ has a weak dependence on the relative momentum q, leading to an excitation that disperses only as q^4.

In Fig. 3(c) we plot the real space density profile corresponding to the d_{xy} mode at $q = 0$. The images are projected onto the $z = 0$ plane and track the time evolution at quarter and half of the oscillation period T. Note that the oscillations are quadrupolar deformations of the density *within* the unit cell such that the mode can support a finite frequency oscillation at zero momentum. This behavior is analogous to optical phonons in polyatomic crystals, which involve relative motion of the atoms within a unit cell.

Dynamical structure factor (DSF).—In order to compare with the experimental INS data, we compute the dynamical structure factor, $S_G(\boldsymbol{q}, \omega) = \text{Im}\langle \delta\rho_G(\boldsymbol{q}, \omega)\delta\rho_{-G}(-\boldsymbol{q}, -\omega)\rangle$. This is readily computed via canonical quantization of the normal modes (see SM [28]), yielding

$$S(\boldsymbol{G}+\boldsymbol{q}, \omega) = \sum_\alpha \frac{\gamma M_{G,\alpha}(\boldsymbol{q})}{2\omega_\alpha(\boldsymbol{q})} \{n(\omega_\alpha)\delta(\omega + \omega_\alpha(\boldsymbol{q}))$$
$$+ [1 + n(\omega_\alpha)]\delta(\omega - \omega_\alpha(\boldsymbol{q}))\}, \quad (4)$$

where $n(\epsilon) = 1/[\exp(\beta\epsilon) - 1]$ is the Bose function, and the matrix element $M_{G,\alpha}(\boldsymbol{q})$ expresses the overlap squared between normal mode α and the density operator. For a given wave vector, only certain normal modes are INS active, while the remaining modes have vanishing $M_{G,\alpha}(\boldsymbol{q})$. This is illustrated in Fig. 2, where INS active (inactive) modes are plotted with solid (dashed) lines. As a check, the DSF analysis predicts that the longitudinal (transverse) acoustic phonon are INS inactive for $\boldsymbol{q}$ vector which are orthogonal (parallel) to the Bragg vector $\boldsymbol{G}$. This

reproduces well-known selection rules of the classical harmonic theory of solids [29]. In addition, our analysis uncovers new selection rules that apply to the gapped modes.

The DSF in Eq. (4) satisfies the sum rule [30]:

$$\int_{-\infty}^{\infty} d\omega\, \omega\, S(\boldsymbol{G} + \boldsymbol{q}, \omega) = \gamma. \quad (5)$$

Hence, although our model contains more phonon modes than predicted by the harmonic theory of solids, their total spectral weight is constrained. In particular, the distinction between a crystal and a CDW is qualitative in nature and, as such, there must be a smooth mechanism by which the amplitude modes disappear as the solid becomes more classical. Indeed, in this limit, the amplitude modes become increasingly energetic, and their spectral weight is accordingly reduced to satisfy the sum rule. As a related observation, if our GL formalism were enlarged to include nonprimary Bragg vectors, more optical modes would appear, but of very high energy and small spectral weight.

Quantum Monte Carlo (QMC) simulation.—We complement the phenomenological GL analysis with an *ab initio* path integral QMC simulation. We model the ^{4}He atoms with the following Hamiltonian:

$$H = -\lambda \sum_{i=1}^{N} \vec{\nabla}_i^2 + \sum_{i<j} V(\boldsymbol{r}_i - \boldsymbol{r}_j), \quad (6)$$

where $\lambda = 6.0596$ Å^2 K for ^{4}He and $V(r)$ is the Aziz potential, which is believed to accurately capture the interatomic potential energy of ^{4}He atoms [31]. We set the simulation parameters to lie within the bcc region of the ^{4}He phase diagram. Explicitly, the temperature is set to $T = 1.6$ K and we consider $N = 2000$ ^{4}He atoms at atomic density $n_0 = 0.02854$ Å^{-3} (molar volume $v_0 = 21.1$ cm^3). The bosonic worldlines configurations are sampled employing the continuous space worm algorithm [32] in the canonical ensemble. Our main observable is the charge susceptibility structure factor evaluated at Matsubara frequency ω_m,

$$\chi(\boldsymbol{q}, i\omega_m) = \frac{1}{N\beta}\left\langle\left|\int_0^\beta d\tau\, e^{i\omega_m\tau}\sum_{i=1}^N e^{i\boldsymbol{q}\cdot\boldsymbol{r}_i(\tau)}\right|^2\right\rangle, \quad (7)$$

where $\boldsymbol{r}_i(\tau)$ denotes the position of the *i*th particle at imaginary time τ.

At finite relative momentum the spectrum is gapped up to the energy scale of the acoustic phonon and hence the dispersion relation can be extracted by fitting the DSF to the asymptotic form $\chi(q, \tau \gg 1/\Delta) \sim f(q, \tau)$, where $f(q, \tau) = A(q)(e^{-\tau\Delta(q)} + e^{-(\beta-\tau)\Delta(q)})$. In addition, we compute the excitation spectrum by performing a numerical analytic continuation on the imaginary time QMC data using the MaxEnt method [33]. We find good

agreement between the excitation spectra computed via these two methods.

We focus on the longitudinal mode along the line connecting the Brillouin zone origin to a primitive Bragg vector. The resulting dispersion relation is depicted in the inset of Fig. 4. For comparison, we also display the experimental INS data [1] and find good agreement with the numerical computation. We were unable to resolve any gapped modes at finite relative momentum. This is likely due to the small spectral weight of the optical mode relative to the acoustic phonons. Experimentally, the ratio is about 1/10. A previous QMC study [34] computed the acoustic dispersion at finite wave vectors, and thus did not detect the optical modes.

To overcome this problem we compute the DSF at a Bragg momentum, where the weight of the acoustic phonons is expected to vanish. To extract the energy scale of the amplitude mode, we fit the imaginary time QMC data to the following form: $\chi(\boldsymbol{G}, \tau \gg 1/\Delta) \sim \chi_0 + f(\boldsymbol{G}, \tau)$. The extensive constant χ_0 takes into account the crystal order parameter. A typical fit of this type is shown in the SM [28]. As before, we also perform numerical analytic continuation of the QMC data and obtain consistent results.

The results of the numerical analytical continuation are presented in the main panel of Fig. 4. We find the spectrum is composed of a gapped resonance peaked at $\omega_H = 0.5(1)$ meV; see also SM [28]. This central result demonstrates numerically the presence of a gapped mode at zero relative momentum in a monoatomic Bravais lattice. Interestingly, this value is smaller than the experimentally measured frequency $\omega_H^{\mathrm{expt}} = 1.2$ meV. Our numerical
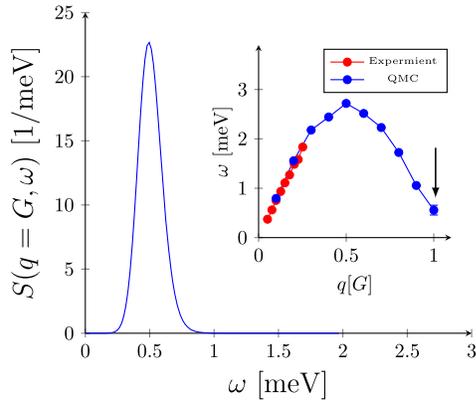
calculation, therefore, predicts an additional and lower energy gapped mode, beyond those found experimentally. Such a mode would have gone undetected, since the experimental setup for the vast majority of existing measurements was not designed to detect phonons with energies below 1 meV [35,36].

Could the experimentally observed optical mode be due to a *two*-phonon process [37]? To assess this possibility, we have analyzed a harmonic lattice model with up to third-neighbor interactions whose parameters are adjusted to match the experimentally observed phonon frequencies at high symmetry points (P, N, and H) in the Brillouin zone [23], and to be stable in the vicinity of the zone center. We thereby obtain a dynamical matrix,

$$\hat{\Phi}^{\alpha\beta}(\boldsymbol{k}) = \sum_{\boldsymbol{R} \neq 0}(1 - \cos \boldsymbol{k} \cdot \boldsymbol{R}) \frac{\partial^2 v(R)}{\partial R^\alpha \partial R^\beta}, \qquad (8)$$

with $\partial_\alpha \partial_\beta v(R) = (\delta^{\alpha\beta} - \hat{R}^\alpha \hat{R}^\beta) R^{-1} v'(R) + \hat{R}^\alpha \hat{R}^\beta v''(R)$. Our model is specified by six parameters, which may be taken to be the values of $v'(R)$ and $v''(R)$ at each of the first three nearest-neighbor distances. We computed the phonon band structure and the dynamic structure factor within this harmonic theory (see SM for details [28]). We find that the peak in the two-phonon contribution to $S(\boldsymbol{G}, \omega)$ lies at a frequency of $\omega_{2\text{-ph}} \simeq 4.3$ meV, and furthermore, the peak amplitude of this two-phonon contribution is 0.6% of the peak value in Fig. 4. We therefore reject this possibility.

Discussion.—Our results motivate future experimental studies of the excitation spectrum of solid ^{4}He. Specifically, it would be interesting to determine the symmetry properties of the gapped modes. Breaking a subgroup of the O_h crystal symmetry group, e.g., by shearing or compressing the lattice, would lift the symmetry enforced degeneracy. The resulting splitting of the phonon branches could be detected in INS experiments.

More broadly, beyond ^{4}He, our analysis may be relevant to other examples of strongly fluctuating quantum solids. In that regard, one promising future theoretical and experimental research direction would be to explore the effect of reduced dimensionality on the amplitude modes such as in the solid phase of two-dimensional dipolar Bose gases [38]. As a concrete prediction, the Lindemann parameter for bcc solid ^{3}He is even larger than that of ^{4}He [16], and therefore we predict that lower energy optical modes should be seen in solid ^{3}He. This would also serve as an experimental confirmation that the optical modes in ^{4}He are strictly due to charge fluctuations and not to gapped fluctuations of the nearby superfluid.

Summarizing, we have identified the gapped modes observed in INS experiments on the bcc phase of solid ^{4}He with amplitude fluctuations of the crystal order. The properties of the gapped modes were analyzed through an effective GL theory and an *ab inito* QMC simulation. In addition, we propose experimental tests for our predictions in solid ^{4}He and quantum solids in general.

FIG. 4.   Dynamical structure factor at the primitive Bragg vector $\boldsymbol{G} = \{1, 1, 0\}$. The spectral function displays a clear resonance at $\omega = 0.5(1)$ meV that we attribute to fluctuation of the CDW order parameter. The first moment, $I_1 = \int d\omega\, \omega\, S(\omega, \boldsymbol{G})$, obeys the f-sum rule $I_1^e = \boldsymbol{G}^2/2m = 2.43$ meV. The numerical value, $I_1^n = 2.6$ meV, deviates by 7% from the exact result. Inset: Dispersion of lowest energy longitudinal excitation computed with QMC simulations (blue), compared to longitudinal acoustic phonon measured in INS experiments (red) [1]. The arrow indicates the optical mode.

[1] T. Markovich, E. Polturak, J. Bossy, and E. Farhi, Phys. Rev. Lett. **88**, 195301 (2002).

[2] O. Pelleg, J. Bossy, E. Farhi, M. Shay, V. Sorkin, and E. Polturak, Phys. Rev. B **73**, 180301 (2006).

[3] O. Pelleg, J. Bossy, E. Farhi, M. Shay, V. Sorkin, and E. Polturak, J. Low Temp. Phys. **151**, 1164 (2008).

[4] O. Pelleg, Ph.D. thesis, Technion-Israel Institute of Technology, 2007.

[5] E. Blackburn, J. Goodkind, S. Sinha, C. Broholm, J. Copley, and R. Erwin, Pramana **71**, 673 (2008).

[6] N. Gov and E. Polturak, Phys. Rev. B **60**, 1019 (1999).

[7] N. Gov, Phys. Rev. B **67**, 052301 (2003).

[8] N. Gov, Phys. Rev. B **62**, 910 (2000).

[9] P. B. Littlewood and C. M. Varma, Phys. Rev. B **26**, 4883 (1982).

[10] D. Sherman, U. S. Pracht, B. Gorshunov, S. Poran, J. Jesudasan, M. Chand, P. Raychaudhuri, M. Swanson, N. Trivedi, A. Auerbach, M. Scheffler, A. Frydman, and M. Dressel, Nat. Phys. **11**, 188 (2015).

[11] D. Podolsky, A. Auerbach, and D. P. Arovas, Phys. Rev. B **84**, 174522 (2011).

[12] S. D. Huber, B. Theiler, E. Altman, and G. Blatter, Phys. Rev. Lett. **100**, 050404 (2008).

[13] M. Endres, T. Fukuhara, D. Pekker, M. Cheneau, P. Schau, C. Gross, E. Demler, S. Kuhr, and I. Bloch, Nature (London) **487**, 454 (2012).

[14] C. Rüegg, B. Normand, M. Matsumoto, A. Furrer, D. F. McMorrow, K. W. Krämer, H. U. Güdel, S. N. Gvasaliya, H. Mutka, and M. Boehm, Phys. Rev. Lett. **100**, 205701 (2008).

[15] A. Travesset, J. Chem. Phys. **141**, 164501 (2014).

[16] H. R. Glyde, *Excitations in Liquid and Solid Helium* (Clarendon Press, Oxford, 1994).

[17] J. G. Dash, Rev. Mod. Phys. **71**, 1737 (1999).

[18] F. W. de Wette, L. H. Nosanow, and N. R. Werthamer, Phys. Rev. **162**, 824 (1967).

[19] T. R. Koehler and N. R. Werthamer, Phys. Rev. A **5**, 2230 (1972).

[20] R. A. Guyer, Solid State Phys. **23**, 413 (1970).

[21] H. R. Glyde, Can. J. Phys. **49**, 761 (1971).

[22] H. Horner, J. Low Temp. Phys. **8**, 511 (1972).

[23] E. B. Osgood, V. J. Minkiewicz, T. A. Kitchens, and G. Shirane, Phys. Rev. A **5**, 1537 (1972).

[24] V. J. Minkiewicz, T. A. Kitchens, G. Shirane, and E. B. Osgood, Phys. Rev. A **8**, 1513 (1973).

[25] S. Aubry, Physica (Amsterdam) **216D**, 1 (2006).

[26] G. Baym, H. A. Bethe, and C. J. Pethick, Nucl. Phys. **A175**, 225 (1971).

[27] S. Alexander and J. McTague, Phys. Rev. Lett. **41**, 702 (1978).

[28] See Supplemental Material at http://link.aps.org/supplemental/10.1103/PhysRevLett.117.085302 for computation of the excitation spectrum and the dynamical structure factor within the GL formalism, classification of the normal modes according to their irreducible representations, extraction of the phonon spectrum from the imaginary time QMC data and calculation of two phonon process contribution to the dynamical structure factor.

[29] M. P. Marder, *Condensed Matter Physics* (John Wiley & Sons, New York, 2010).

[30] The familiar f-sum rule is $\int d\omega\, \omega S(\bm{k}, \omega) = k^2/2m$, where m is the particle mass. For $\bm{k} = \bm{G} + \bm{q}$ with $q \ll G$, the rhs of the sum rule is $G^2/2m + \mathcal{O}(q)$, and is approximately a constant, which we can use to fix the coefficient γ of the time derivative in our Lagrangian density.

[31] R. A. Aziz, V. P. S. Nain, J. S. Carley, W. L. Taylor, and G. T. McConville, J. Chem. Phys. **70**, 4330 (1979).

[32] M. Boninsegni, N. V. Prokof'ev, and B. V. Svistunov, Phys. Rev. E **74**, 036701 (2006).

[33] M. Jarrell and J. Gubernatis, Phys. Rep. **269**, 133 (1996).

[34] V. Sorkin, E. Polturak, and J. Adler, Phys. Rev. B **71**, 214304 (2005).

[35] Because of the finite resolution of INS experiments, at low frequency and small momentum transfer, the dynamical structure factor is contaminated by spurious spectral weight originating from the strong elastic Bragg scattering. See, for example, the discussion on "Bragg tails" in Ref. [39] and experimental data in Ref. [1].

[36] E. Polturak (private communication).

[37] This possibility was suggested to us by B. I. Halperin (private communication).

[38] H. P. Büchler, E. Demler, M. Lukin, A. Micheli, N. Prokof'ev, G. Pupillo, and P. Zoller, Phys. Rev. Lett. **98**, 060404 (2007).

[39] G. Shirane, S. M. Shapiro, and J. M. Tranquada, *Neutron Scattering with a Triple-Axis Spectrometer* (Cambridge University Press, Cambridge, England, 2002).